Article

Current Biology

Circadian Regulation of Cochlear Sensitivity to Noise by Circulating Glucocorticoids

Graphical Abstract

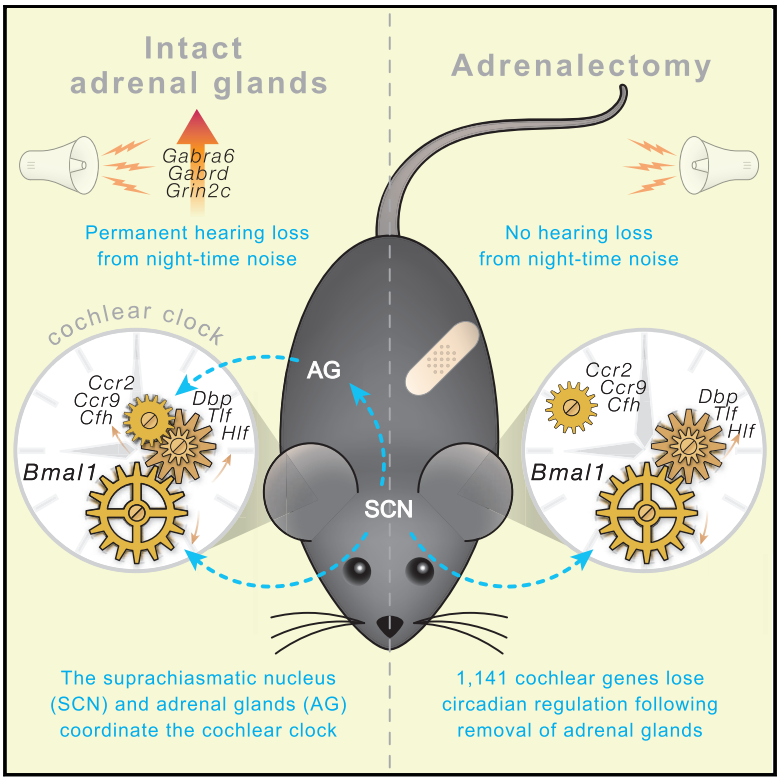

Highlights

- Core clock gene expression in the cochlea depends on SCN input
- *Bmal1* is essential to maintain cochlear clock function
- Differential noise sensitivity is regulated by glucocorticoid-dependent signals
- Chronopharmacological approaches will optimize the treatment of hearing disorders

Authors

Christopher R. Cederroth, Jung-sub Park, Vasiliki Basinou, ..., Nadir Kadri, Frédéric Gachon, Barbara Canlon

Correspondence

christopher.cederroth@ki.se

In Brief

How is the cochlear clock regulated? Cederroth, Park et al. show that circadian rhythms in the cochlea are controlled by the suprachiasmatic nucleus and glucocorticoids from the adrenal glands that act as major regulators of the differential sensitivity to day and night noise trauma.

Cederroth et al., 2019, Current Biology *29*, 2477–2487
August 5, 2019
https://doi.org/10.1016/j.cub.2019.06.057

CellPress

Current Biology
Article

Circadian Regulation of Cochlear Sensitivity to Noise by Circulating Glucocorticoids

Christopher R. Cederroth,[1,8,9,*] Jung-sub Park,[1,6,8] Vasiliki Basinou,[1,8] Benjamin D. Weger,[4] Evangelia Tserga,[1] Heela Sarlus,[1] Anna K. Magnusson,[2] Nadir Kadri,[3] Frédéric Gachon,[4,5,7] and Barbara Canlon[1]
[1]Department of Physiology and Pharmacology, Karolinska Institutet, Stockholm 17177, Sweden
[2]Department of Clinical Science Intervention and Technology, Karolinska Institutet, Stockholm 17177, Sweden
[3]Department of Laboratory Medicine, Karolinska Institutet, Stockholm 17177, Sweden
[4]Department of Diabetes and Circadian Rhythms, Nestlé Institute of Health Sciences, 1015 Lausanne, Switzerland
[5]School of Life Sciences, Ecole Polytechnique Fédérale de Lausanne, 1015 Lausanne, Switzerland
[6]Department of Otolaryngology, Ajou University School of Medicine, 164, Worldcup-ro, Yeongtong-gu, Suwon 16499, Korea
[7]Present address: Institute for Molecular Bioscience, The University of Queensland, St. Lucia, QLD 4072, Australia
[8]These authors contributed equally
[9]Lead Contact
*Correspondence: christopher.cederroth@ki.se
https://doi.org/10.1016/j.cub.2019.06.057

SUMMARY

The cochlea possesses a robust circadian clock machinery that regulates auditory function. How the cochlear clock is influenced by the circadian system remains unknown. Here, we show that cochlear rhythms are system driven and require local *Bmal1* as well as central input from the suprachiasmatic nuclei (SCN). SCN ablations disrupted the circadian expression of the core clock genes in the cochlea. Because the circadian secretion of glucocorticoids (GCs) is controlled by the SCN and GCs are known to modulate auditory function, we assessed their influence on circadian gene expression. Removal of circulating GCs by adrenalectomy (ADX) did not have a major impact on core clock gene expression in the cochlea. Rather it abolished the transcription of clock-controlled genes involved in inflammation. ADX abolished the known differential auditory sensitivity to day and night noise trauma and prevented the induction of GABA-ergic and glutamate receptors mRNA transcripts. However, these improvements were unrelated to changes at the synaptic level, suggesting other cochlear functions may be involved. Due to this circadian regulation of noise sensitivity by GCs, we evaluated the actions of the synthetic glucocorticoid dexamethasone (DEX) at different times of the day. DEX was effective in protecting from acute noise trauma only when administered during daytime, when circulating glucocorticoids are low, indicating that chronopharmacological approaches are important for obtaining optimal treatment strategies for hearing loss. GCs appear as a major regulator of the differential sensitivity to day or night noise trauma, a mechanism likely involving the circadian control of inflammatory responses.

INTRODUCTION

Disruptions in the regulation of circadian rhythms are known to affect a large number of bodily functions, including sleep, metabolism, and inflammatory responses [1]. The mammalian circadian clock system is organized hierarchically with the bilateral suprachiasmatic nuclei (SCN) of the hypothalamus being the master clock that orchestrates physiological functions of all peripheral organs through neuroendocrine and autonomic nervous systems [2, 3]. When the SCN is ablated, oscillations in peripheral tissues become asynchronous [4]. Although light is the main synchronizer of the SCN clock, other cues, like feeding, locomotor activity, temperature, and hormonal factors, can synchronize peripheral clocks. Hormones under strict circadian control, such as glucocorticoids (GCs), have been shown to entrain peripheral organs [3, 5] and become arrhythmic in the absence of the SCN [6–9]. GCs are among the most potent synchronizers of peripheral clocks [10, 11] through interactions with the core clock proteins [12, 13].

The core clock system consists of autoregulatory transcriptional and translational feedback loops that regulate clock-controlled genes for specific physiological outputs [1]. Disruption of clock genes (*Per*, *Cry*, *Clock*, *Bmal1*, *Rev-erbβ*, and *Ror*) in mice is known to generate a variety of phenotypes [14]. In particular, disruption of *Bmal1* has the greatest impact on clock rhythms and mutants lacking *Bmal1* display a wide array of disorders, including arrhythmic locomotor activity in constant darkness [15], arthropathy [16], infertility [17, 18], symptoms of the metabolic syndrome [19, 20], reduced B cell production [21], and decreased lifespan [22], overall highlighting its important role for the maintenance of homeostasis.

Recently, a robust self-sustained clock was identified in the cochlea, with ample circadian expression of core clock genes, such as *Per1*, *Per2*, *Bmal1*, and *Rev-erbα*, and persistent oscillations of the PER2::LUC reporter *ex vivo* [23]. PER2 is abundantly expressed in hair cells and spiral ganglion neurons, the primary cells for auditory transmission [23]. A greater sensitivity to night noise trauma was found compared to daytime and coincided with a peak expression of *Per2* at night [23]. What drives

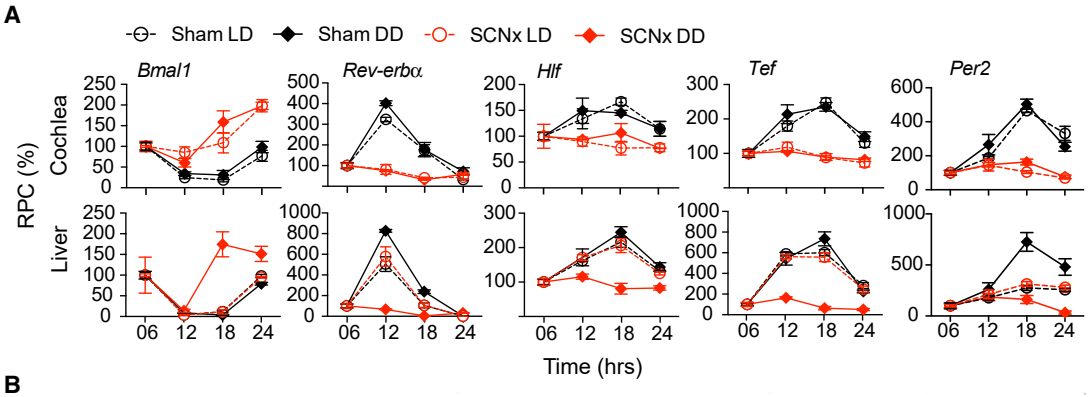

B

	Cochlea					Liver				
	Bmal1	*Rev-erbα*	*Hlf*	*Tef*	*Per2*	*Bmal1*	*Rev-erbα*	*Hlf*	*Tef*	*Per2*
Time	**<0,0001**	**<0,0001**	**0,0144**	**<0,0001**	**<0,0001**	**<0,0001**	**<0,0001**	**<0,0001**	**<0,0001**	**<0,0001**
Light	0,2134	0,0579	0,6149	0,442	0,2788	**0,0016**	0,3378	**0,0012**	**<0,0001**	0,0586
SCN	**<0,0001**	**<0,0001**	**<0,0001**	**<0,0001**	**<0,0001**	**0,0003**	**<0,0001**	**<0,0001**	**<0,0001**	**<0,0001**
Time x Light	0,2108	0,1867	0,9435	0,6549	0,072	**0,0021**	0,0665	0,0562	**<0,0001**	**0,0396**
Time x SCN	**<0,0001**	**<0,0001**	**0,0115**	**<0,0001**	**<0,0001**	**0,0005**	**<0,0001**	**0,0002**	**<0,0001**	**<0,0001**
Light x SCN	0,7379	0,057	0,4789	0,4051	0,7601	**<0,0001**	**<0,0001**	**<0,0001**	**<0,0001**	**<0,0001**
Time x Light x SCN	0,2469	0,2311	0,3517	0,3711	0,1595	**0,0008**	**<0,0001**	**0,001**	**<0,0001**	**<0,0001**

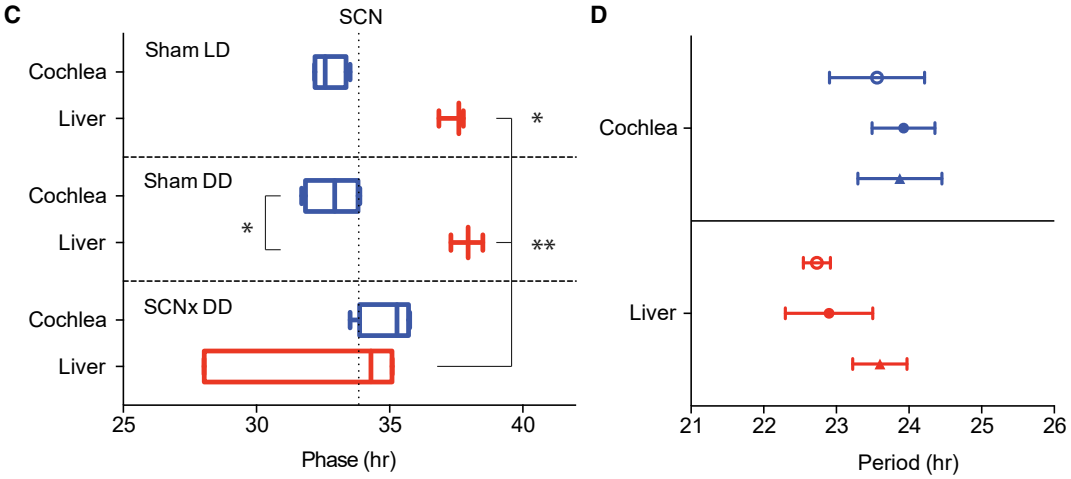

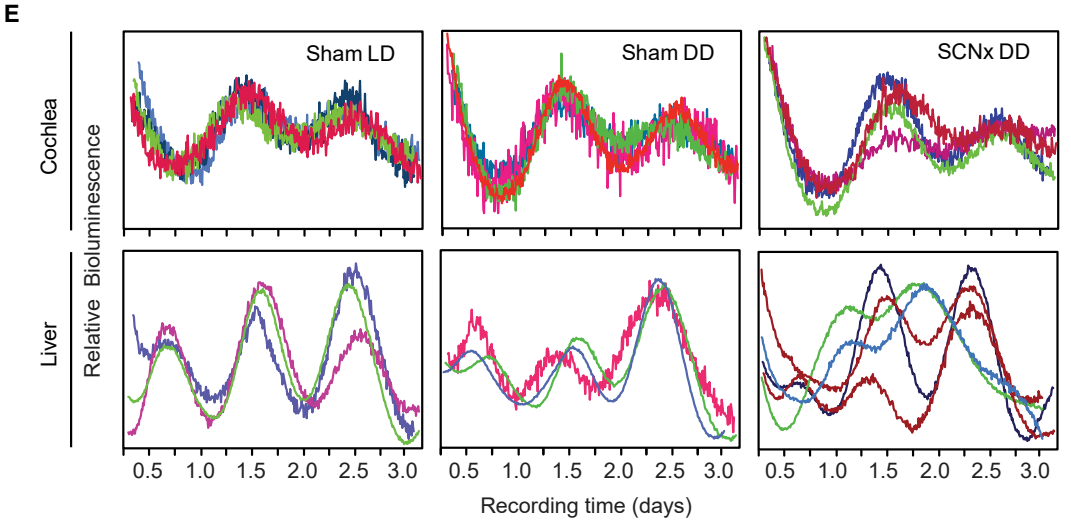

(legend on next page)

the cochlear rhythms and the differential sensitivity to noise throughout the day remains unknown. In a series of pharmacological and surgical experiments, GCs have been shown to modulate auditory function in response to noise insults [24, 25] and thus could potentially integrate with the cochlear clock to regulate the differential sensitivity to noise.

Here, we investigate whether BMAL1 and the SCN influence cochlear clock rhythms and whether systemic cues, such as GCs, regulate the differential day versus night noise sensitivity. We hypothesize that GCs regulate cochlear clock rhythms on a subset of circadian genes that may influence the vulnerability to noise trauma at specific times of the day.

RESULTS

Cochlear Circadian Rhythms Are Dependent on Input from the SCN

To directly determine whether the SCN is required for sustained rhythmicity in the cochlea, we performed bilateral SCN electrolytic lesioning (SCNx), which is considered a reliable method to demonstrate the control of the SCN over peripheral organs [26]. Ablation of the SCN was confirmed by histology, various metabolic measures (e.g., O_2 consumption [VO_2], respiratory exchange rate [RER], and food intake), and circadian locomotor activity (Figures S1A–S1K). In the cochlea, the circadian expression of clock and clock-controlled genes (i.e., *Bmal1*, *Per2*, *Rev-erbα*, *Hlf*, and *Tef*) was abolished in SCNx samples in both LD and dark/dark (DD) conditions. In contrast, the circadian rhythm of these genes in the liver of SCNx animals was only abolished in DD conditions (Figure 1A). Three-way ANOVA statistics reflected these differences between the liver and the cochlea (Figure 1B). This result suggests that, in contrast to the liver, light can entrain the cochlear clock through signals from the SCN, as already shown for the adrenal gland [9]. Interestingly, the effects on the liver followed the regulation of fecal corticosterone (CORT), which remained rhythmic in SCNx mice in LD, but not in DD cycles (Figure S1L). These findings are consistent with previous reports showing persisting fecal CORT secretion in behaviorally arrhythmic *Syt10:Cre;Bmal1(fx/fx)* mice [27], unlike what is known for blood CORT (most likely deriving from the adrenal glands), which is completely arrhythmic in SCNx animals in LD [6]. Consistent with the systemic adaptation to jet lag, qualitative observations show the circadian pattern of cochlear mRNA transcripts of *Bmal1*, *Per2*, *Rev-erbα*, and *Rev-erbβ* to be inverted after 3 weeks in an inverted dark-light cycle, similar to what was evidenced in the liver, a highly rhythmic circadian tissue used as a control (Figure S1M).

We next assessed the impact of SCN ablation on liver and cochlear PER2 rhythms *ex vivo* (Figures 1C–1E) using PER2::LUC transgenic mice [4, 28]. It is well known that placing an organ in culture can reset its clock machinery, even when rhythmicity is lacking *in vivo* due to the lack of SCN input [26]. Consistently, cochleas and liver from SCNx mice showed ample rhythms *ex vivo*, even though no longer present *in vivo* (Figure 1). Livers from SCNx mice placed in constant darkness (DD) showed a high dispersion of phase times, with a phase advance up to 5 h when compared to sham DD livers ($p = 0.002$; Figures 1C and 1E). In contrast, SCNx did not trigger phase differences in the cochleae ($p = 0.26$; Figures 1C and 1E), and phase synchrony was maintained. Period was not affected by either SCN ablation or manipulation of light-dark cycle in both the cochlea ($p = 0.885$) and liver ($p = 0.319$; Figure 1D). The phase differences in the liver and the cochlea did not correlate with the period values (cochlea, $R^2 = 0.0024$, $p = 0.879$; liver, $R^2 = 0.1843$, $p = 0.184$). Overall, our results indicate that the influences of the SCN on the cochlea differ from those on the liver.

The Cochlear Clock Requires Bmal1

BMAL1 function was deleted in the cochlea by using *Pax2-Cre* mice (*Pax2:Cre* or *Cre*). As *Pax2-Cre* is also expressed in the female germline (A. Groves, personal communication), oocytes were expected to contribute with an excised floxed allele, which is thus deleted (Δ). Hence, homozygous *Bmal1(fx/fx);Pax2:Cre* are referred as *cBmal1(fx/Δ)*, carrying one constitutively deleted allele and one floxed allele only targeted in Cre-expressing cells (here, the cochlea). *cBmal1(wt/wt)* were used as controls. Actograms confirmed that whole-body rhythmicity from *cBmal1(fx/Δ)* was indistinguishable from controls in both LD and DD conditions (Figure S2). We took advantage of the *cBmal1(fx/Δ)* mice to cross them and obtain full *cBmal1(Δ/Δ)* mutants that served as a positive control for the systemic loss of circadian rhythmicity. Similar to constitutive *Bmal1* knockout (KO) mice [29], *cBmal1(Δ/Δ)* mice were completely arrhythmic (Figure S2). Overall, the lack of systemic effects of the *cBmal1(fx/Δ)* mice allowed us to investigate the effects of *Bmal1* loss of function specifically in the cochlea. Cochleae from *cBmal1(fx/Δ)* showed a rhythmic PER2::LUC oscillation but with a rapid loss of rhythmicity, in contrast to the SCN or the liver that kept sustained rhythmicity (Figure 2). As what would be expected from mice constitutively lacking *Bmal1*, *cBmal1(Δ/Δ)* confirmed the absence of PER2::LUC rhythmicity in all organs (Figure 2). The rhythmic but dampening PER2::LUC oscillations in *cBmal1(fx/Δ)*, but not in *cBmal1(Δ/Δ)*, suggest that the cochlear clock is systems driven and influenced by the input of other zeitgebers [30]. These

Figure 1. Effects of SCN Ablation on Clock Gene Expression in the Cochlea and the Liver *In Vivo* and *Ex Vivo*

(A) Nanostring nCounter assays on cochlear and liver mRNA samples from sham (black) and SCNx (red) mice collected every 6th hour around the clock in normal LD cycles (open circles) and in DD cycles (filled diamonds). Values are expressed in relative percentage change (RPC). Values are mean ± SEM; n = 3.

(B) Summary statistics of the three-way ANOVA with circadian time (time), light/dark cycle (light), and SCN lesioning (SCN) as factors and their interactions ($\alpha = 0.05$).

(C) Peak phase time of PER2::LUC cochlear (blue) and liver (red) samples *ex vivo* is shown as boxplots. The median value (vertical line inside the box) with the lower and upper quartiles shown as horizontal lines and the whiskers defining the endpoints is shown. The average peak phase time of intact SCN in LD is illustrated with the vertical dotted line, which is used as a reference point. Note the sham-LD cochlea is significantly phase advanced in relation to the SCN.

(D) Periods of PER2::LUC cochlear (blue) and liver (red) samples are not affected by SCN lesioning or light-dark cycles. Results are mean values ± SEM; n = 4. *$p < 0.05$; **$p < 0.01$; one-way ANOVA with Sidak's post hoc analysis.

(E) Individual bioluminescent recordings from PER2::LUC cochleae (above) or liver (below) samples from sham LD, sham DD, or SCNx DD conditions.

See also Figure S1.

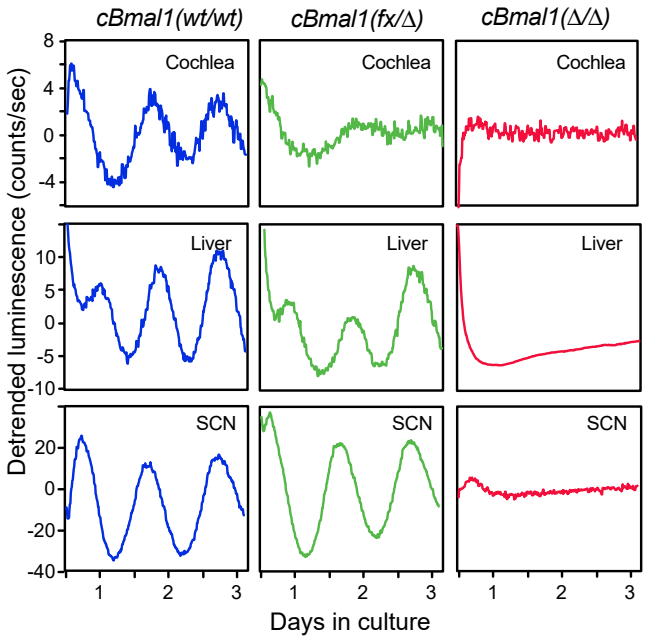

Figure 2. Cochlear-Specific *Bmal1* Deletion (*cBmal1*) Abolishes Circadian Rhythms in the Cochlea *Ex Vivo*

Representative bioluminescent traces from *cBmal1;PER2::LUC* mice showing normal PER2::LUC oscillations in *(wt/wt)* cochleae, whereas these rapidly dampen in the *(fx/Δ)* explants, but not in the liver or the SCN. *cBmal1(Δ/Δ)* show complete loss of PER2::LUC rhythmicity in all tissues tested. See also Figure S2.

findings show that the cochlear clock relies on *Bmal1* for maintaining a self-sustained clock in absence of compensatory mechanisms.

Glucocorticoid Depletion Protects the Cochlea against Night Noise Trauma

We next evaluated the contribution of endogenous GCs, established downstream mediators of SCN input [31], on day versus night noise sensitivity and on circadian gene expression. A surgical model of GC depletion (adrenalectomy [ADX]) was applied, resulting in a loss of the circadian pattern of plasma CORT in ADX mice compared to sham-operated mice ($p < 0.0001$ at the peak expression time; Figure 3A). We also confirmed the loss of rhythmicity of *Fkbp5*, *Lpin1*, and *Gk* in the liver from ADX mice (ANOVA for Sham and ADX data showed a significant effect of group, $p = 0.0003–0.0001$, and a highly significant interaction between surgical condition and time of sample collection, $p < 0.0001$, for the three genes; Figure 3B). These liver genes have been shown to be most affected in their circadian rhythmicity after adrenalectomy [32].

To explore the influence of GCs on time-dependent auditory function, we exposed animals to noise (6–12 kHz; 100 dB sound pressure level [SPL] for 1 h) during daytime or nighttime. This noise paradigm does not cause morphological changes to the outer hair cells [23]. ADX did not affect the threshold shifts 24 h after day ($p = 0.47$) or night noise exposure ($p = 0.56$; Figure 3C). However, 2 weeks after night noise exposure, ADX animals improved their hearing at all frequencies when compared to sham-operated mice that displayed persisting hearing loss ($p < 0.0009$; Figure 3A), but a significant threshold shift of 7–16 dB remained. The day-noise-exposed, sham-operated controls recovered, as did the ADX mice ($p > 0.83$; Figure 3C), consistent with Meltser et al. [23]. Wave 1 amplitudes of the auditory brainstem response (ABR) were not altered at either 16 or 24 kHz or the wave 1/5 ratio (data not shown). At the synaptic level, we found a similar decrease in the number of ribbons after day or night noise exposure at 3.4- and 4.5-mm distance from the apex when compared to unexposed controls, but ADX did not rescue the loss of ribbons (Figure 3D). Quantification of ribbon size did not reveal any difference among all groups across all frequencies (data not shown). These findings suggest that the surge of GCs plays a significant role in the vulnerability to noise trauma at nighttime, without obvious morphological or functional effects on pre-synaptic ribbons.

We next performed RNA sequencing (RNA-seq) on whole cochleae collected 2 h after day or night noise trauma to investigate potential mechanisms involved in the regulation of noise sensitivity by GCs. Using a generalized linear model (STAR Methods), we identified 15 genes whose induction by noise was significant at nighttime in sham-operated animals and was abolished in cochleae from ADX mice (Figure S3; Table S1; Data S1). These genes are involved in neurotransmitter signaling, such as *Gabrd*, *Gabra6*, and *Grin2C*, which have been previously reported to have functional responses in the cochlea via GABA and NMDA receptors [33, 34]. The induction of neuronal genes that have shown their importance during auditory neuronal development (i.e., *Neurod1* and *Neurod2*) [35] was also suppressed in ADX mice after night noise trauma (Figure S3). *Car4*, which encodes the carbonic anhydrase 4, is abundantly expressed in the lateral wall and in inner and outer hair cells [36] and showed a similar gene expression pattern (Figure S3). Additional genes were identified (Figure S3) but whose function in the ear is presently unknown. On the other hand, ADX did not prevent the induction of genes after day noise exposure. Overall, our data indicate that GCs regulate a subset of genes that are triggered only at nighttime and that ADX abolishes their induction.

Glucocorticoids Regulate the Circadian Expression of Inflammatory Genes in the Cochlea

To further explore the molecular mechanisms involved in the circadian regulation of noise sensitivity, we performed RNA-seq around the clock in sham-operated and ADX cochleae to identify all the rhythmic genes under GC control. We next applied a harmonic linear-regression-based model selection approach on cochlear RNA-seq data that allows the clustering of genes depending on their rhythmic or constant expression patterns [37]. This approach assigned genes to one of five models with distinct rhythmic patterns and phase specificity (Figure 4A). Model 1 is composed of genes that are non-rhythmic in ADX and sham conditions (7,174 genes); model 2 is composed of non-rhythmic genes in sham cochleae that gained rhythmicity after ADX (455 genes); model 3 identifies rhythmic genes in both ADX and sham conditions (5,941 genes); model 4 consists of genes with altered rhythmicity after ADX (altered phase and amplitude; 129 genes); and model 5 consists of rhythmic genes that lost their rhythmicity in ADX conditions

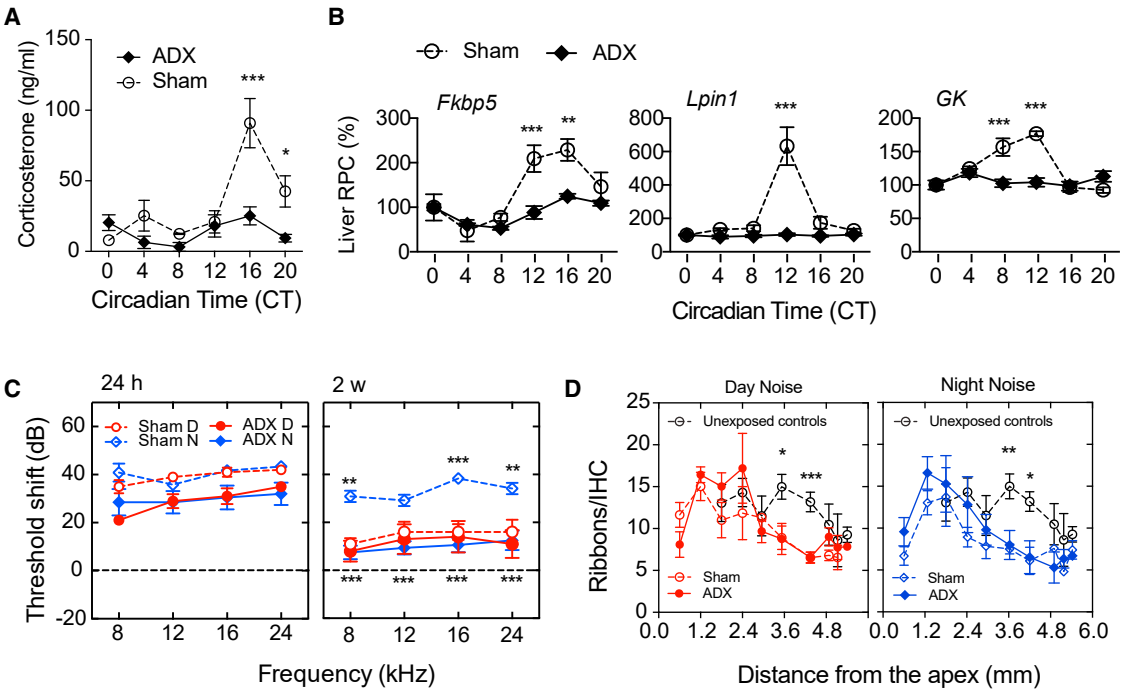

Figure 3. Endogenous GCs Regulate Sensitivity to Night Noise Trauma without Influencing Synaptic Ribbons

(A) Plasma levels of circulating corticosterone (CORT) in sham-operated (open circles) and ADX (filled diamonds) mice every 4th hour across the circadian cycle.

(B) Nanostring nCounter assays show mRNA expression levels of three GC-dependent liver genes in sham (open circles) and ADX (filled diamonds) animals. All values are expressed in relative percentage change (RPC) using CT 0 values as reference.

Values are mean ± SEM; n = 3–7 (A); n = 3 (B). *p < 0.05; **p < 0.01; ***p < 0.001; two-way ANOVA with Sidak's post hoc analysis.

(C) ABR threshold shifts from sham-operated (open symbols) and ADX (filled symbols) mice exposed to noise at 9 a.m. (day, red circles) or at 9 p.m. (night, blue diamonds) were measured 24 h (left panel) and 2 weeks (right panel) post-exposure. Results are mean values ± SEM; n = 5–8. *p < 0.05; **p < 0.01; ***p < 0.001; two-way ANOVA with Bonferroni post hoc analysis. Stars depicted above sham-operated, night-noise-exposed group denote significance against sham-operated, day-noise-exposed, whereas starts shown below indicate statistical significance between ADX night-exposed and sham-operated, night-exposed mice.

(D) Quantification of synaptic ribbons along the cochleae of ADX (filled symbols) and sham mice (open symbols) exposed to a day (left panel, red circles) or a night (right panel, blue diamonds) noise trauma. Open black circles represent unexposed controls used as a reference. Results are mean values ± SEM; n = 2–7—with the exception of n = 1 for some basal measurements. *p < 0.05; **p < 0.01; ***p < 0.001; one-way ANOVA with Sidak post hoc analysis for each frequency region. See also Figure S3 and Table S1.

(1,141 genes). This analysis revealed that the rhythmicity of 22.5% of the rhythmic genes depends on GCs (model 5; Figure 4B). Gene Ontology (GO) analysis of the five models using PANTHER according to Mi et al. [38] is shown in Figure S4A. To further examine these differences, we searched for over- or under-representation of genes using a statistical overrepresentation test (PANTHER; see STAR Methods for details). In model 2, we found an overrepresentation of genes related to RNA metabolic processes and DNA-dependent transcription (approximately 1.8-fold enrichment; Table S1). Genes in model 2 (gain of mRNA rhythmicity) were mainly related to transcriptional processes. Model 4, which defines rhythmic genes with altered phase and amplitude after ADX, was enriched in clock-related genes (30-fold enrichment; Table S2; Figure S4B). Genes in model 4 (rhythmic mRNAs but with altered properties) were strongly associated with the circadian system and showed a wide-range distribution of mRNA phases. Model 5 (loss of rhythmicity) shows enrichment of genes related to the immune system, suggesting that rhythmic genes under the control of circulating GCs regulate circadian inflammatory responses in the cochlea (see also Tables S2 and S3).

Genes involved in the differential circadian regulation of noise sensitivity were predicted to appear in model 5, whereby the removal of circulating GCs would lead to the loss of circadian transcription in the cochlea. A deeper GO analysis of model 5 identified genes encoding for defense and immune proteins, immunoglobulin receptors, cell adhesion molecules, and extracellular matrix proteins (Figure S4C; Table S3). GO analysis revealed that biological processes related to the immune system were the most enriched and included genes with a Bayesian information criterion weight (BICW) score >0.9 [37] with a clear loss of rhythmicity in ADX conditions, such as cluster of differentiation 109 (*Cd109*) and C-C chemokine receptor type 2 and 9 (*Ccr2* and *Ccr9*; Figure 4C; Table S3). ANOVA then confirmed a significant effect of group and time of sample collection ($p < 0.02$ in all cases). With lower BICW scores, additional genes controlled by circulating GCs belonging to GO terms, such as antibacterial response, cytokine receptors, defense and immunity, immunoglobulin receptor family, interferon family, and response to stress, were found (Table S3). Overall, the results from the GO analysis suggest that pro-inflammatory signals rise at nighttime in the cochlea, when noise sensitivity is greatest.

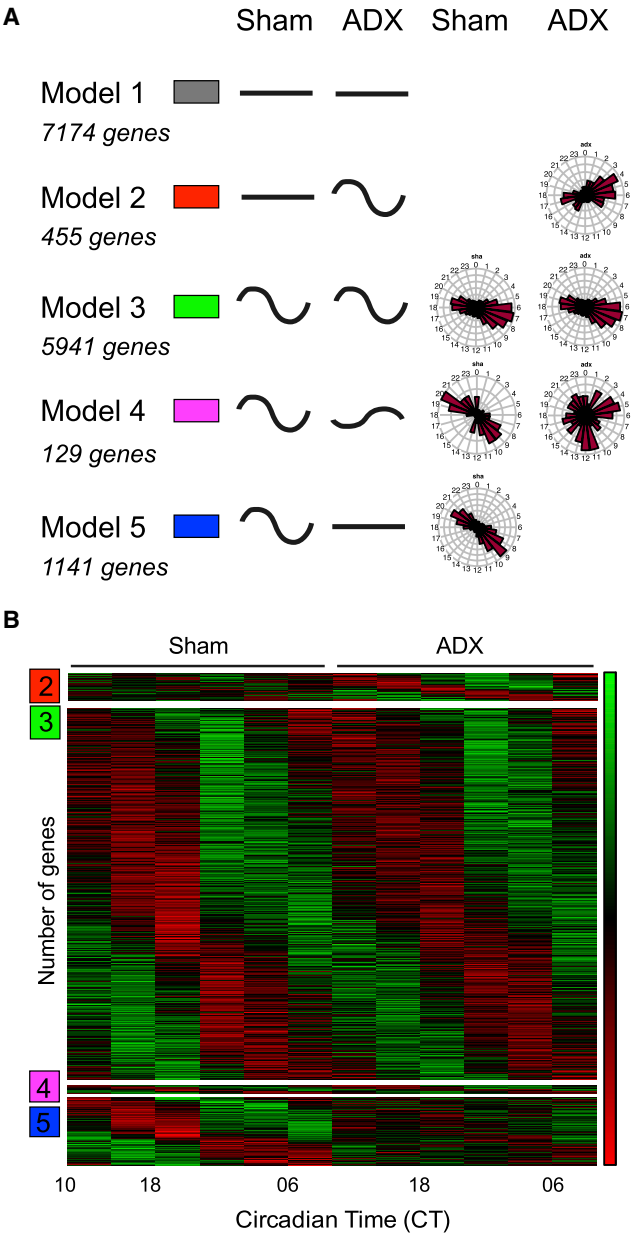

Figure 4. Transcriptomic Analysis of the Rhythmic Regulation of the Cochlear Gene Expression by GCs

(A) Clustering of genes obtained from the RNA-seq depending on their rhythmic or constant patterns of expression between sham and ADX conditions and the corresponding number of genes. Model 1, constant mRNA levels in both conditions; model 2, constant mRNA levels that became rhythmic in ADX conditions; model 3, rhythmic mRNA levels in both conditions; model 4, rhythmic transcripts that retained their rhythmicity but showed altered amplitude and phase properties; and model 5, rhythmic transcripts that lost their rhythmicity in ADX conditions are shown. Phase distribution of the five different models is shown on the right panel.

(B) Expression heatmap for the gene groups showing rhythmic mRNA levels in at least one of the conditions (sham operated or ADX). Mean relative expression of 3 biological replicates is shown (green, low levels; red, high levels). Model 1 was excluded from the heatmap; none of the genes were circadian and would result in a black area, yielding no information.

(C) Transcriptional profile of three putative GC-dependent circadian cochlear genes from model 5, which were no longer rhythmic after adrenalectomy. mRNA levels in sham-operated samples (open circles-dashed lines) and in ADX samples (black diamonds-full lines).

All values are expressed in relative percentage change (RPC) using circadian time (CT) 0 values as reference (n = 3). The horizontal axis shows CT. Values are mean ± SEM; n = 3 (C). *p < 0.05; **p < 0.01; two-way ANOVA with Sidak's post hoc analysis.

See also Figure S4 and Tables S2 and S3.

Differential Effects of Dexamethasone (DEX) on Cochlear Rhythms and Noise Trauma

Thus far, the present data indicate that GCs might be pro-inflammatory in the cochlea at nighttime, resulting in an increased vulnerability to noise. This is counter-intuitive because it is rather well established that DEX, a synthetic GR agonist, is protective to the ear [24, 25]. However, all of these experiments were performed during daytime, when the endogenous GC levels are low. We therefore hypothesized that the effectiveness of DEX on the cochlea may rely on the time of the day when administered. We first examined the actions of DEX on cochlear PER2::LUC rhythms when applied at trough or at peak PER2 expression in presence or absence of forskolin pre-synchronization (Figure 5A), after selecting the optimal dose during day treatment (Figure 5B). In absence of pre-synchronization, both day and night treatment with DEX increased PER2::LUC amplitude ($p < 0.0001$), but a phase advance was only observed at night time ($p = 0.049$). No effects on the period were found (Figures 5C–5E). In order to differentiate the actions of DEX from its synchronizing effects, we pre-synchronized cochleae using forskolin 2 days after being placed in culture. Day treatment increased the amplitude of the PER2::LUC rhythm by 60% ($p = 0.0004$), whereas night treatment decreased the amplitude by 50% ($p = 0.01$; Figure 5F). These findings illustrate that DEX has a differential effect on the pre-synchronized cochlear rhythms, depending on the time of the day. In pre-synchronized cochleae, the phase was not affected after DEX treatment (Figure 5G), whereas an increase in period was only found after night treatment (Figure 5H). After day and night treatment, RU486, a GR antagonist, blocked the effects of DEX; however, a decreased amplitude change was found after day treatment (Figures S5A and S5B). The reasons for these differences are not known. Spironolactone, a mineralocorticoid receptor (MR) antagonist, did not alter the changes induced by DEX on cochlear clock rhythms ($p = 0.83$; $n = 3–12$), further confirming the specificity of GR. We used liver samples as a comparison and found that DEX had no day or night effects on amplitude changes with or without forskolin pre-synchronization (Figures S5C and S5F). However, differential effects were seen on phase and period (Figures S5D, S5E, S5G, and S5H). These findings illustrate that the clocks from the cochlea and the liver respond differently to the actions of DEX in presence or absence of pre-synchronization.

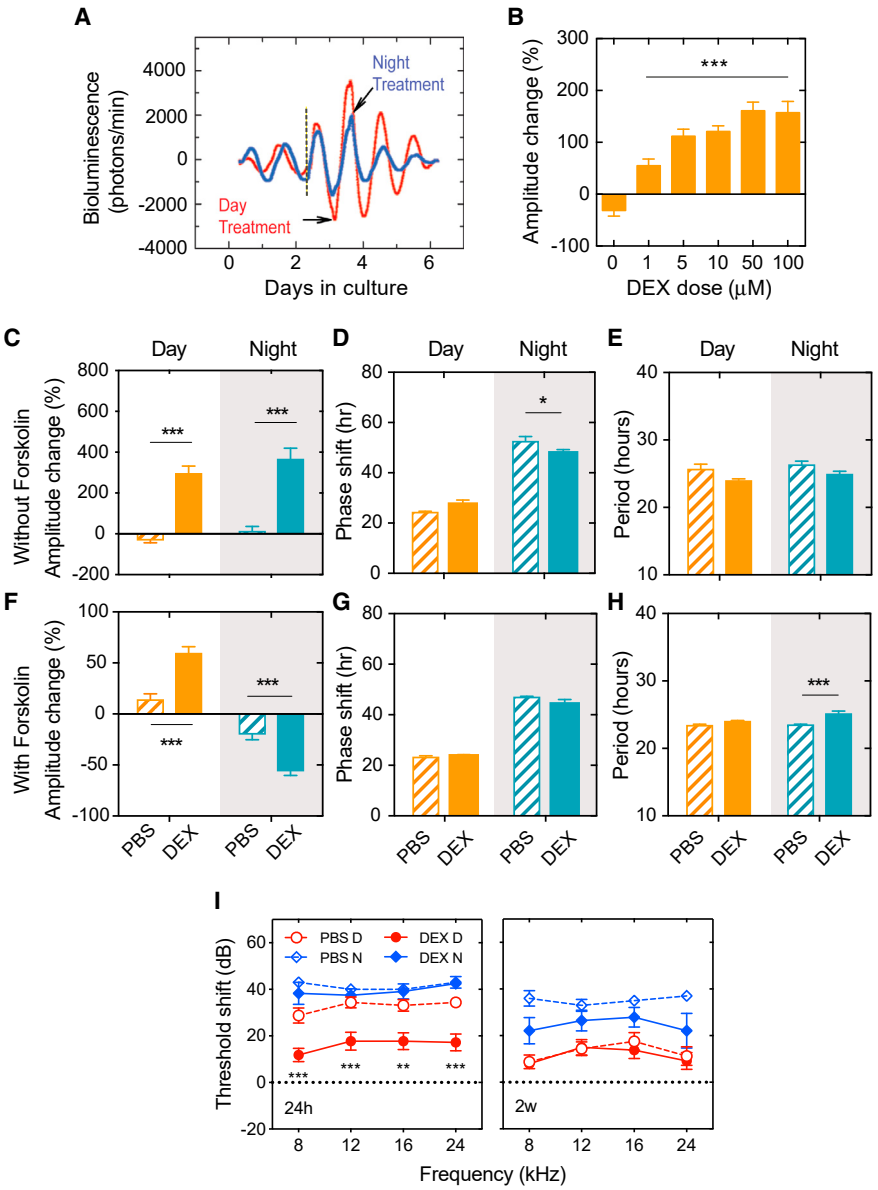

Figure 5. GC Protection against Noise Trauma Correlates with Changes in the Cochlear Clock Machinery

(A) Representative detrended bioluminescence records of isolated PER2::LUC cochleae treated with DEX at the trough (day, red) or at the peak (night, blue) of oscillations. Forskolin synchronization was performed on day 3 at the rise of the oscillations (black dashed line) before DEX treatment. The time of forskolin treatment is shown in dashed black lines.

(B) Dexamethasone dose response in PER2::LUC amplitude changes from cochleas *ex vivo* expressed as a percent change from pre-treatment values (treatment at 9 a.m.). 5 μM was selected for subsequent treatments because it showed significant increases in amplitude changes at non-saturating levels.

(C–H) Quantification of PER2::LUC amplitude, phase, and period change after DEX treatment of cochleae in absence (C–E) or presence (F–H) of forskolin pre-treatment (day, orange filled bars; night, green filled bars). PBS treatment is shown with hatched bars. Gray shaded areas indicate the nighttime.

(I) Auditory threshold shifts of mice treated with PBS (open symbols) and DEX (filled symbols) exposed to noise at 9 a.m. (day, red circles) or at 9 p.m. (night, blue diamonds) and measured 24 h post-exposure (left) and 2 weeks post-exposure (right). For the sake of clarity, we only indicate the statistics of DEX versus PBS groups for day or night noise exposure, respectively.

Results are mean values ± SEM; n = 3–5 (A); n = 5–6 (C–E); n = 8–21 (F–H); n = 5–11 (I). **p < 0.01; ***p < 0.001; two-way ANOVA with Bonferroni post hoc analysis. D, day; N, night. See also Figure S5.

The differential responses of the cochlear clock to day or night DEX treatment *ex vivo* indicate that GC actions on the auditory system might differ between day and night *in vivo*. To test this, mice were treated with DEX 90 min prior to day or night noise trauma. At 24 h post-exposure, the DEX day treatment protected against noise damage compared to the day PBS-treated group (DEX day, 12–18 dB; PBS, 29–34 dB; $p < 0.01$ for all frequencies tested; Figure 5I). On the contrary, no effect of DEX treatment was observed 24 h after night noise exposure (37–43 dB for both DEX and PBS; $p > 0.83$ for all frequencies tested; Figure 5I). 2 weeks post-noise trauma, no differences were found between PBS- and DEX-treated animals exposed during the day. Similarly, DEX treatment did not improve the thresholds from animals exposed to noise at nighttime. Still, the PBS day-exposed mice showed lower threshold shifts than the night-noise-exposed animals (ANOVA data showed a significant effect of group; $p < 0.0001$), confirming the differential sensitivity to day and night noise injury in the control animals. These findings illustrate that the protective effects of DEX occur when administered during the day (when GC levels are low), with significant changes seen 24 h post-noise exposure, indicating time-specific effects of steroid treatment against noise-induced hearing loss.

DISCUSSION

The present findings confirm that cochlear rhythms are controlled by *Bmal1* and suggest this control is systems driven through signals from the SCN. When *Bmal1* is deleted *in vivo* in a tissue-specific manner, a number of additional cues could contribute to a sustained circadian clock. In absence of a functional BMAL1 in the whole body, or in absence of the SCN, there are no more cyclic cues to drive cellular clocks *in vivo*, and this is likely why the cochlear rhythms become arrhythmic. Such hierarchical relationship between the SCN and the cochlea has never been evidenced before. Interestingly, the influence of the SCN on cochlear rhythms differed from the liver, being associated with circulating CORT levels.

The ADX effect, which protected mice from hearing damage following noise exposure at night, is a main result of this study. Two hours after night noise exposure, cochlear genes such as *Gabra6*, *Gabrd*, and *Grin2c* were upregulated in sham-operated animals, but not in ADX mice. *Grin2c* transcripts, which encode the NMDA receptor subunit 2C, are expressed in the rodent cochlea [33]. Because glutamate is considered as the main neurotransmitter between inner hair cells (IHCs) and afferent neurons and that NMDA receptors are known to induce cochlear excitotoxicity [39], it is possible that acute excitotoxicity contributes to the reduced hearing thresholds observed 2 weeks after night noise exposure. However, in spite of these clear molecular mechanisms, our electrophysiological and morphological analyses of the inner hair cell and afferent neuron synapse did not reveal any obvious change when assessed 2 weeks post-noise exposure. It is possible that, in spite of significant molecular changes, these may not have reached a sufficient amplitude to cause morphological changes.

We note, however, that the ribbon quantification presented here differs from that of our previous report [23], where a lower number of synaptic ribbons were found in the apical region from sham-exposed mice. The study from Meltser et al. relied on ImageJ and manual thresholding, which may have underestimated the ribbons from that region compared to the present study that uses Imaris, resulting in a more accurate estimate of ribbon counts and similar to what has been reported by Kujawa and Liberman [40]. Meltser et al. showed a clear involvement of neurotrophins in the vulnerability to night noise trauma, whereby activation of the tropomyosin receptor kinase B (TrkB) rescued the loss of hearing after night noise trauma and partially recovered the amount of ribbons lost [23]. Instead, the present findings show that ADX partially rescues ABR thresholds from night noise trauma but without altering the number of ribbons, suggesting that the GC-mediated differential sensitivity to day and night noise trauma is independent from synaptic ribbon loss. Indeed, Yuan et al. showed that >85% loss of IHC-afferent synapses is required to cause a decrease of >10 dB in the ABR thresholds. Our attempts to assess synapse pairing (i.e., how many ribbons are paired with a postsynaptic entity) using GluR2 antibodies failed, as the success of this staining is variable and thus the status of functional synapses in ADX model remains uncovered. Overall, these results indicate that the differential sensitivity to noise throughout the day involves additional mechanisms yet to be identified. For instance, this could involve outer hair cell, spiral ganglion neuron, or lateral wall function, which have not yet been explored.

The use of different models and mouse strains in the present study suggests that the differential sensitivity to noise could be universal. However, differential day and night noise vulnerability has never been tested *in vivo* in the PER2::LUC and *cBmal1(fx/Δ)* mice from a C57BL/6J background. Recent studies suggest that the circadian sensitivity to noise might not apply to all mice strains and rodent species or to all types of noise trauma [41, 42]. Thus, differences in timing (when and how long), intensity (low or high noise levels), and genetic background may impact the outcome. Indeed, our findings strongly support the involvement of GCs in the circadian sensitivity to noise trauma. In this regard, the amplitude of the circadian CORT profile is known to differ between rat strains, stress levels, pathogenic conditions, and sex [43]. We therefore hypothesize that the differential sensitivity to noise at different times of the day may correlate with the amplitude of the circadian CORT profile and the response to stress [43].

GCs are well-established downstream mediators of SCN input [31]. Our data strongly suggest that GCs could be one of the key signals that regulate sensitivity to noise at different times of the day. It is interesting to discuss the role of GCs in the regulation of pro-inflammatory signals within the cochlea together with the recent finding, which showed the presence of immune cells (mainly monocytes) in the cochlea of postnatal mice [44]. Monocytes, which develop in the bone marrow, express CCR2 at their surface and migrate to sites of inflammation in response to CCL2 [45]. We found that mRNA expression of *Ccr2* is rhythmic in the whole cochlea, with an increase at nighttime 4 h after GC levels have peaked in the plasma. Interestingly, GCs have been shown to enhance the migratory capacity of monocytes [46] and regulate their secretion of the complement factor H [47], which we also found to be rhythmic in the cochlea. Whether GCs trigger greater mobilization of monocytes from the bone marrow during nighttime or whether they influence monocytes known to patrol tissue [48] is an interesting question. Sautter et al. revealed that noise sensitivity and subsequent monocyte migration remains unaffected in *Ccr2* KO mice [49], suggesting that other factors may compensate for CCR2 loss of function. It is also possible that mice were exposed to noise during daytime, which could have left the potential involvement of CCR2 in monocyte migration unrevealed. Indeed, monocytes also express in certain conditions other chemokine receptors, such as CCR9 [50], which encoding gene was also found circadian in the cochlea and dependent on circulating GC levels. Thus, consistent with the findings that *Ccr2* and *Ccr9* rhythmicity in the cochlea is abolished after ADX, it is reasonable to speculate that GCs would contribute to a greater migration of monocytes into the cochlea after a noise trauma delivered at nighttime, which in turn would have a negative impact on auditory recovery. The other possibility is that GCs regulate the recruitment of other immune cells into the cochlea. For instance, other cell types, like NK cells, NKT cells, or T cells, are known to express CCR2 and CCR9 [51] and thus could be recruited to the cochlea in a GC-dependent manner. Our data thus suggest that GCs affect the transcriptional regulation of inflammatory signals within the cochlea, but the RNA-seq data from samples collected 2 h after noise trauma did not reveal differentially regulated inflammatory signals between day and night. It is possible that the chosen time point is not appropriate to reveal such potential changes or that sampling the whole cochlea dilutes more subtle effects occurring in sub-compartments that could not be evidenced in the present study.

Nonetheless, the collected evidence strongly suggests that mice are more sensitive to noise trauma during the night because GCs predispose the cochlea to inflammation. This contrasts the known assumption that GCs would be beneficial to the auditory system. There are indeed multiple findings in humans and rodents, suggesting that GCs act on the hearing system to modulate sensitivity to noise, either positively or negatively [24, 25]. Chronic stress has been shown to increase the susceptibility of rats to noise trauma [52], whereas acute stress is protective [53, 54]. Although it is established that chronic exposure to high levels of circulating GCs is potentially harmful to the inner ear, it is rather unexpected to find that the daily surge in GCs levels at nighttime aggravates the cochlear response to noise. As a

consequence, changes in GCs may result in completely opposite fates in the vulnerability or resilience to noise trauma. Our former studies on the protective effects of restrained stress on noise trauma showed that auditory protection was achieved in the same mouse strain during daytime when plasma CORT levels were 2-fold higher than what was found in the present study at nighttime [53, 54]. Such findings are in line with the well-established non-monotonic dose responses commonly found with hormones [55]. Thus, the effects of GCs on the cochlea appear to be affected by dose, duration, and time of administration. A careful evaluation of all these parameters may help to better understand the actions of glucocorticoids on the inner ear.

The most commonly used agents to treat hearing disorders are a class of GC steroids, such as DEX and prednisolone [56]. Here, the protective effects of DEX against noise trauma were evidenced 24 h post-noise exposure and coincided when circulating CORT levels were low. In contrast, the administration of DEX at the time when circulating GCs were high did not protect against noise trauma. One of the reasons for the differential protective response to DEX treatment against noise trauma could stem from differences in local bioavailability in the cochlea due to differences in the permeability of the blood labyrinth barrier, as it happens in the brain [57]. Assuming that local DEX levels are similar after day or night administration, GR activity might thus differ depending on the time of the day. Such opposite fates in DEX responses are illustrated by the different changes in PER2::LUC amplitudes in cochlear explants, increasing when cochleae are treated during daytime and decreasing when treated during nighttime. In support of this hypothesis, the transcriptional activity of GR is controlled in a circadian manner by circadian regulators [13]. Thus, the anti-inflammatory actions of DEX might prove ineffective, even though it has a high potency, at the onset of night. Interestingly, the effects of DEX treatment on amplitude and phase differed between the cochlea and the liver. In the context of SCN ablations, our data also show differences between the two tissues *in vivo* and *in vitro*. These findings indicate that the chronopharmacological actions of DEX could likely differ, depending on the target tissue. Overall, in order to achieve the desired effects of steroid treatment against noise-induced hearing loss, the time of administration should be taken under careful consideration. The inappropriate timing of steroid administration against hearing loss could be grounds to the mixed success described in clinical trials [58, 59].

STAR★METHODS

Detailed methods are provided in the online version of this paper and include the following:

- KEY RESOURCES TABLE
- LEAD CONTACT AND MATERIALS AVAILABILITY
- EXPERIMENTAL MODEL AND SUBJECT DETAILS
- METHOD DETAILS
  - Adrenalectomy
  - Corticosterone measurement
  - Suprachiasmatic nucleus ablations
  - Actograms
  - Organotypic cultures
  - Drug treatment *in vivo* and *in vitro*
  - Acoustic trauma and auditory brainstem response (ABR)
  - Immunocytochemistry and quantification of synaptic elements
  - mRNA extraction
  - Quantitative evaluation of mRNA transcripts
  - RNA-sequencing
  - Noise exposure RNA-seq analysis
  - Temporal RNA-seq analysis
  - Gene ontology analysis
- QUANTIFICATION AND STATISTICAL ANALYSIS
- DATA AND CODE AVAILABILITY

SUPPLEMENTAL INFORMATION

Supplemental Information can be found online at https://doi.org/10.1016/j.cub.2019.06.057.

ACKNOWLEDGMENTS

We thank John Hogenesch for insightful comments on this manuscript. We also thank the iGE3 platform at the University of Geneva for technical support on the RNA sequencing and Nanostring experiments. We thank Dr. Joseph S. Takahashi for the PER2::LUC transgenic mouse, Dr. Christopher Bradfield for the *Bmal1* floxed mice, Dr. Gabriella Lundkvist for insightful discussions, Drs. Juleen Zierath and Anna Krook for allowing us to use their metabolic cages (CLAMS), and Lars E. Gustafsson for his helpful advice regarding the electrolytic lesions. We thank all the members of the Canlon laboratory for technical assistance, in particular Dr. Rocio Moreno Paublete for assistance with sample collection around the clock. This study was mainly funded by Communication Disorders of the NIH R21DC013172 and 1R56DC016415-01 (B.C.) and the Swedish Medical Research Council K2014-99X-22478-01-3 (B.C.). Additional funds were obtained from Knut and Alice Wallenberg Foundation (B.C.; no. KAW2008), the National Institute on Deafness and other National Research Foundation of Korea grant (2014R1A6A3A03058661) funded by the Ministry of Education of the Korean Government (J.-s.P.), Karolinska Institutet (B.C. and C.R.C.), Tysta Skolan (B.C., J.-s.P., and C.R.C.), Hörselforskningsfonden (B.C. and C.R.C.), Magnus Bergvalls (C.R.C.), and the European Union's Horizon 2020 research and innovation programme under the Marie Skłodowska-Curie grant agreement no. 722046 (C.R.C.) [60]. B.C. and C.R.C. also received funding from the Office of the Assistant Secretary of Defense for Health Affairs, through the Neurosensory and Rehabilitation under award no. W81XWH-16-1-0032. Opinions, interpretations, conclusions, and recommendations are those of the author and are not necessarily endorsed by the Department of Defense.

AUTHOR CONTRIBUTIONS

C.R.C., J.-s.P., and V.B. contributed equally as first authors to this work. C.R.C., J.-s.P., V.B., E.T., and B.C. performed *ex vivo* experiments; C.R.C., J.-s.P., V.B., and B.C. performed *in vivo* experiments; B.D.W. and F.G. conducted the temporal RNA-seq analyses; C.R.C., J.-s.P., V.B., and E.T. analyzed data and performed statistical analysis; C.R.C., J.-s.P., V.B., and B.C. conceived experiments; C.R.C. was responsible for the genetic models; A.K.M., H.S., and N.K. helped to develop the scientific arguments and contributed to data interpretation; C.R.C., J.-s.P., and B.C. wrote the manuscript; and all authors contributed to its editing.

DECLARATION OF INTERESTS

B.D.W. and F.G. were employees of Nestlé Institute of Health Sciences SA. All other authors declare no competing interests.

Received: July 20, 2018
Revised: May 21, 2019
Accepted: June 20, 2019
Published: July 25, 2019

REFERENCES

1. Bass, J., and Takahashi, J.S. (2010). Circadian integration of metabolism and energetics. Science *330*, 1349–1354.
2. Kalsbeek, A., Perreau-Lenz, S., and Buijs, R.M. (2006). A network of (autonomic) clock outputs. Chronobiol. Int. *23*, 521–535.
3. Mohawk, J.A., Green, C.B., and Takahashi, J.S. (2012). Central and peripheral circadian clocks in mammals. Annu. Rev. Neurosci. *35*, 445–462.
4. Yoo, S.H., Yamazaki, S., Lowrey, P.L., Shimomura, K., Ko, C.H., Buhr, E.D., Siepka, S.M., Hong, H.K., Oh, W.J., Yoo, O.J., et al. (2004). PERIOD2:LUCIFERASE real-time reporting of circadian dynamics reveals persistent circadian oscillations in mouse peripheral tissues. Proc. Natl. Acad. Sci. USA *101*, 5339–5346.
5. Challet, E. (2015). Keeping circadian time with hormones. Diabetes Obes. Metab. *17* (*Suppl 1*), 76–83.
6. Moore, R.Y., and Eichler, V.B. (1972). Loss of a circadian adrenal corticosterone rhythm following suprachiasmatic lesions in the rat. Brain Res. *42*, 201–206.
7. Radziuk, J.M. (2013). The suprachiasmatic nucleus, circadian clocks, and the liver. Diabetes *62*, 1017–1019.
8. Stephan, F.K., and Zucker, I. (1972). Circadian rhythms in drinking behavior and locomotor activity of rats are eliminated by hypothalamic lesions. Proc. Natl. Acad. Sci. USA *69*, 1583–1586.
9. Ishida, A., Mutoh, T., Ueyama, T., Bando, H., Masubuchi, S., Nakahara, D., Tsujimoto, G., and Okamura, H. (2005). Light activates the adrenal gland: timing of gene expression and glucocorticoid release. Cell Metab. *2*, 297–307.
10. Cuesta, M., Cermakian, N., and Boivin, D.B. (2015). Glucocorticoids entrain molecular clock components in human peripheral cells. FASEB J. *29*, 1360–1370.
11. Dickmeis, T. (2009). Glucocorticoids and the circadian clock. J. Endocrinol. *200*, 3–22.
12. Balsalobre, A., Brown, S.A., Marcacci, L., Tronche, F., Kellendonk, C., Reichardt, H.M., Schütz, G., and Schibler, U. (2000). Resetting of circadian time in peripheral tissues by glucocorticoid signaling. Science *289*, 2344–2347.
13. Lamia, K.A., Papp, S.J., Yu, R.T., Barish, G.D., Uhlenhaut, N.H., Jonker, J.W., Downes, M., and Evans, R.M. (2011). Cryptochromes mediate rhythmic repression of the glucocorticoid receptor. Nature *480*, 552–556.
14. Ko, C.H., and Takahashi, J.S. (2006). Molecular components of the mammalian circadian clock. Hum. Mol. Genet. *15*, R271–R277.
15. Bunger, M.K., Wilsbacher, L.D., Moran, S.M., Clendenin, C., Radcliffe, L.A., Hogenesch, J.B., Simon, M.C., Takahashi, J.S., and Bradfield, C.A. (2000). Mop3 is an essential component of the master circadian pacemaker in mammals. Cell *103*, 1009–1017.
16. Bunger, M.K., Walisser, J.A., Sullivan, R., Manley, P.A., Moran, S.M., Kalscheur, V.L., Colman, R.J., and Bradfield, C.A. (2005). Progressive arthropathy in mice with a targeted disruption of the Mop3/Bmal-1 locus. Genesis *41*, 122–132.
17. Alvarez, J.D., Hansen, A., Ord, T., Bebas, P., Chappell, P.E., Giebultowicz, J.M., Williams, C., Moss, S., and Sehgal, A. (2008). The circadian clock protein BMAL1 is necessary for fertility and proper testosterone production in mice. J. Biol. Rhythms *23*, 26–36.
18. Boden, M.J., Varcoe, T.J., Voultsios, A., and Kennaway, D.J. (2010). Reproductive biology of female Bmal1 null mice. Reproduction *139*, 1077–1090.
19. Lamia, K.A., Storch, K.F., and Weitz, C.J. (2008). Physiological significance of a peripheral tissue circadian clock. Proc. Natl. Acad. Sci. USA *105*, 15172–15177.
20. Marcheva, B., Ramsey, K.M., Buhr, E.D., Kobayashi, Y., Su, H., Ko, C.H., Ivanova, G., Omura, C., Mo, S., Vitaterna, M.H., et al. (2010). Disruption of the clock components CLOCK and BMAL1 leads to hypoinsulinaemia and diabetes. Nature *466*, 627–631.
21. Sun, Y., Yang, Z., Niu, Z., Peng, J., Li, Q., Xiong, W., Langnas, A.N., Ma, M.Y., and Zhao, Y. (2006). MOP3, a component of the molecular clock, regulates the development of B cells. Immunology *119*, 451–460.
22. Kondratov, R.V., Kondratova, A.A., Gorbacheva, V.Y., Vykhovanets, O.V., and Antoch, M.P. (2006). Early aging and age-related pathologies in mice deficient in BMAL1, the core componentof the circadian clock. Genes Dev. *20*, 1868–1873.
23. Meltser, I., Cederroth, C.R., Basinou, V., Savelyev, S., Lundkvist, G.S., and Canlon, B. (2014). TrkB-mediated protection against circadian sensitivity to noise trauma in the murine cochlea. Curr. Biol. *24*, 658–663.
24. Canlon, B., Meltser, I., Johansson, P., and Tahera, Y. (2007). Glucocorticoid receptors modulate auditory sensitivity to acoustic trauma. Hear. Res. *226*, 61–69.
25. Meltser, I., and Canlon, B. (2011). Protecting the auditory system with glucocorticoids. Hear. Res. *281*, 47–55.
26. Tahara, Y., Kuroda, H., Saito, K., Nakajima, Y., Kubo, Y., Ohnishi, N., Seo, Y., Otsuka, M., Fuse, Y., Ohura, Y., et al. (2012). In vivo monitoring of peripheral circadian clocks in the mouse. Curr. Biol. *22*, 1029–1034.
27. Husse, J., Leliavski, A., Tsang, A.H., Oster, H., and Eichele, G. (2014). The light-dark cycle controls peripheral rhythmicity in mice with a genetically ablated suprachiasmatic nucleus clock. FASEB J. *28*, 4950–4960.
28. Park, J.S., Cederroth, C.R., Basinou, V., Meltser, I., Lundkvist, G., and Canlon, B. (2016). Identification of a circadian clock in the inferior colliculus and its dysregulation by noise exposure. J. Neurosci. *36*, 5509–5519.
29. Rakai, B.D., Chrusch, M.J., Spanswick, S.C., Dyck, R.H., and Antle, M.C. (2014). Survival of adult generated hippocampal neurons is altered in circadian arrhythmic mice. PLoS ONE *9*, e99527.
30. Kornmann, B., Schaad, O., Bujard, H., Takahashi, J.S., and Schibler, U. (2007). System-driven and oscillator-dependent circadian transcription in mice with a conditionally active liver clock. PLoS Biol. *5*, e34.
31. Son, G.H., Chung, S., and Kim, K. (2011). The adrenal peripheral clock: glucocorticoid and the circadian timing system. Front. Neuroendocrinol. *32*, 451–465.
32. Oishi, K., Amagai, N., Shirai, H., Kadota, K., Ohkura, N., and Ishida, N. (2005). Genome-wide expression analysis reveals 100 adrenal gland-dependent circadian genes in the mouse liver. DNA Res. *12*, 191–202.
33. Ruel, J., Chabbert, C., Nouvian, R., Bendris, R., Eybalin, M., Leger, C.L., Bourien, J., Mersel, M., and Puel, J.L. (2008). Salicylate enables cochlear arachidonic-acid-sensitive NMDA receptor responses. J. Neurosci. *28*, 7313–7323.
34. Maison, S.F., Rosahl, T.W., Homanics, G.E., and Liberman, M.C. (2006). Functional role of GABAergic innervation of the cochlea: phenotypic analysis of mice lacking GABA(A) receptor subunits alpha 1, alpha 2, alpha 5, alpha 6, beta 2, beta 3, or delta. J. Neurosci. *26*, 10315–10326.
35. Jahan, I., Kersigo, J., Pan, N., and Fritzsch, B. (2010). Neurod1 regulates survival and formation of connections in mouse ear and brain. Cell Tissue Res. *341*, 95–110.
36. Okamura, H.O., Sugai, N., Suzuki, K., and Ohtani, I. (1996). Enzyme-histochemical localization of carbonic anhydrase in the inner ear of the guinea pig and several improvements of the technique. Histochem. Cell Biol. *106*, 425–430.
37. Atger, F., Gobet, C., Marquis, J., Martin, E., Wang, J., Weger, B., Lefebvre, G., Descombes, P., Naef, F., and Gachon, F. (2015). Circadian and feeding rhythms differentially affect rhythmic mRNA transcription and translation in mouse liver. Proc. Natl. Acad. Sci. USA *112*, E6579–E6588.
38. Mi, H., Muruganujan, A., Casagrande, J.T., and Thomas, P.D. (2013). Large-scale gene function analysis with the PANTHER classification system. Nat. Protoc. *8*, 1551–1566.
39. Pujol, R., Puel, J.L., Gervais d'Aldin, C., and Eybalin, M. (1993). Pathophysiology of the glutamatergic synapses in the cochlea. Acta Otolaryngol. *113*, 330–334.
40. Kujawa, S.G., and Liberman, M.C. (2009). Adding insult to injury: cochlear nerve degeneration after "temporary" noise-induced hearing loss. J. Neurosci. *29*, 14077–14085.

41. Harrison, R.T., and Bielefeld, E.C. (2018). Little evidence for a chronotolerance effect for impulse noise exposure in the C57BL/6J mouse. Neurosci. Lett. *684*, 127–131.
42. Sheppard, A., Liu, X., Alkharabsheh, A., Chen, G.D., and Salvi, R. (2019). Intermittent low-level noise causes negative neural gain in the inferior colliculus. Neuroscience *407*, 135–145.
43. Lightman, S.L., and Conway-Campbell, B.L. (2010). The crucial role of pulsatile activity of the HPA axis for continuous dynamic equilibration. Nat. Rev. Neurosci. *11*, 710–718.
44. Matern, M., Vijayakumar, S., Margulies, Z., Milon, B., Song, Y., Elkon, R., Zhang, X., Jones, S.M., and Hertzano, R. (2017). Gfi1^{Cre} mice have early onset progressive hearing loss and induce recombination in numerous inner ear non-hair cells. Sci. Rep. *7*, 42079.
45. Tsou, C.L., Peters, W., Si, Y., Slaymaker, S., Aslanian, A.M., Weisberg, S.P., Mack, M., and Charo, I.F. (2007). Critical roles for CCR2 and MCP-3 in monocyte mobilization from bone marrow and recruitment to inflammatory sites. J. Clin. Invest. *117*, 902–909.
46. Yeager, M.P., Pioli, P.A., Collins, J., Barr, F., Metzler, S., Sites, B.D., and Guyre, P.M. (2016). Glucocorticoids enhance the in vivo migratory response of human monocytes. Brain Behav. Immun. *54*, 86–94.
47. Lemercier, C., Julen, N., Coulpier, M., Dauchel, H., Ozanne, D., Fontaine, M., and Ripoche, J. (1992). Differential modulation by glucocorticoids of alternative complement protein secretion in cells of the monocyte/macrophage lineage. Eur. J. Immunol. *22*, 909–915.
48. Yang, J., Zhang, L., Yu, C., Yang, X.F., and Wang, H. (2014). Monocyte and macrophage differentiation: circulation inflammatory monocyte as biomarker for inflammatory diseases. Biomark. Res. *2*, 1.
49. Sautter, N.B., Shick, E.H., Ransohoff, R.M., Charo, I.F., and Hirose, K. (2006). CC chemokine receptor 2 is protective against noise-induced hair cell death: studies in CX3CR1(+/GFP) mice. J. Assoc. Res. Otolaryngol. *7*, 361–372.
50. Schmutz, C., Cartwright, A., Williams, H., Haworth, O., Williams, J.H., Filer, A., Salmon, M., Buckley, C.D., and Middleton, J. (2010). Monocytes/macrophages express chemokine receptor CCR9 in rheumatoid arthritis and CCL25 stimulates their differentiation. Arthritis Res. Ther. *12*, R161.
51. Griffith, J.W., Sokol, C.L., and Luster, A.D. (2014). Chemokines and chemokine receptors: positioning cells for host defense and immunity. Annu. Rev. Immunol. *32*, 659–702.
52. Canlon, B., Erichsen, S., Nemlander, E., Chen, M., Hossain, A., Celsi, G., and Ceccatelli, S. (2003). Alterations in the intrauterine environment by glucocorticoids modifies the developmental programme of the auditory system. Eur. J. Neurosci. *17*, 2035–2041.
53. Tahera, Y., Meltser, I., Johansson, P., Hansson, A.C., and Canlon, B. (2006). Glucocorticoid receptor and nuclear factor-kappa B interactions in restraint stress-mediated protection against acoustic trauma. Endocrinology *147*, 4430–4437.
54. Tahera, Y., Meltser, I., Johansson, P., and Canlon, B. (2006). Restraint stress modulates glucocorticoid receptors and nuclear factor kappa B in the cochlea. Neuroreport *17*, 879–882.
55. Joëls, M. (2006). Corticosteroid effects in the brain: U-shape it. Trends Pharmacol. Sci. *27*, 244–250.
56. Wei, B.P., Stathopoulos, D., and O'Leary, S. (2013). Steroids for idiopathic sudden sensorineural hearing loss. Cochrane Database Syst. Rev. (7), CD003998.
57. Pan, W., and Kastin, A.J. (2017). The blood-brain barrier: regulatory roles in wakefulness and sleep. Neuroscientist *23*, 124–136.
58. Trune, D.R., and Canlon, B. (2012). Corticosteroid therapy for hearing and balance disorders. Anat. Rec. (Hoboken) *295*, 1928–1943.
59. Rauch, S.D. (2008). Clinical practice. Idiopathic sudden sensorineural hearing loss. N. Engl. J. Med. *359*, 833–840.
60. Schlee, W., Hall, D.A., Canlon, B., Cima, R.F.F., de Kleine, E., Hauck, F., Huber, A., Gallus, S., Kleinjung, T., Kypraios, T., et al. (2018). Innovations in doctoral training and research on tinnitus: the European School on Interdisciplinary Tinnitus Research (ESIT) perspective. Front. Aging Neurosci. *9*, 447.
61. Johnson, B.P., Walisser, J.A., Liu, Y., Shen, A.L., McDearmon, E.L., Moran, S.M., McIntosh, B.E., Vollrath, A.L., Schook, A.C., Takahashi, J.S., and Bradfield, C.A. (2014). Hepatocyte circadian clock controls acetaminophen bioactivation through NADPH-cytochrome P450 oxidoreductase. Proc. Natl. Acad. Sci. USA *111*, 18757–18762.
62. Franklin, K.B.J., and Paxinos, G. (2008). The Mouse Brain (Elsevier).
63. Park, J.S., Cederroth, C.R., Basinou, V., Sweetapple, L., Buijink, R., Lundkvist, G.B., Michel, S., and Canlon, B. (2017). Differential phase arrangement of cellular clocks along the tonotopic axis of the mouse cochlea ex vivo. Curr. Biol. *27*, 2623–2629.e2.
64. Vikhe Patil, K., Canlon, B., and Cederroth, C.R. (2015). High quality RNA extraction of the mammalian cochlea for qRT-PCR and transcriptome analyses. Hear. Res. *325*, 42–48.
65. Flicek, P., Ahmed, I., Amode, M.R., Barrell, D., Beal, K., Brent, S., Carvalho-Silva, D., Clapham, P., Coates, G., Fairley, S., et al. (2013). Ensembl 2013. Nucleic Acids Res. *41*, D48–D55.
66. Dobin, A., Davis, C.A., Schlesinger, F., Drenkow, J., Zaleski, C., Jha, S., Batut, P., Chaisson, M., and Gingeras, T.R. (2013). STAR: ultrafast universal RNA-seq aligner. Bioinformatics *29*, 15–21.
67. Love, M.I., Huber, W., and Anders, S. (2014). Moderated estimation of fold change and dispersion for RNA-seq data with DESeq2. Genome Biol. *15*, 550.
68. Weger, B.D., Weger, M., Görling, B., Schink, A., Gobet, C., Keime, C., Poschet, G., Jost, B., Krone, N., Hell, R., et al. (2016). Extensive regulation of diurnal transcription and metabolism by glucocorticoids. PLoS Genet. *12*, e1006512.

STAR★METHODS

KEY RESOURCES TABLE

REAGENT or RESOURCE	SOURCE	IDENTIFIER
Chemicals, Peptides, and Recombinant Proteins		
D-luciferin potassium salt	Promega	Cat# E1602
Forskolin	Sigma-Aldrich	Cat# F3917
Dexamethasone	Sigma-Aldrich	Cat# D-1159
RU486 (Mifepristone)	Sigma-Aldrich	Cat# M-8046
Spironolactone	Sigma-Aldrich	Cat# S-3378
Ketaminol (50 mg/ml)	Intervet	Cat# 511485
Rompun (20 mg/ml)	Bayer A/S	Cat# KP0A43D
Mouse Anti-CtBP2 (1:200)	BD-Biosciences	Cat# 612044; RRID: AB_399431
Rabbit anti-Myosin VIIa (1:200)	Proteus Biosciences	Cat#25-6790; RRID: AB_10015251
IgG2a goat anti-mouse AF488 (1:500)	ThermoFisher Scientific	Cat#A21131; RRID: AB_2535771
IgG donkey anti-rabbit AF647 (1:200)	ThermoFisher Scientific	Cat#557783; RRID: AB_2536183
IgG1 goat anti-mouse AF568 (1:500)	ThermoFisher Scientific	Cat#A21124; RRID: AB_2535766
TRIC-conjugated goat anti-mouse	Jackson Immunoresearch	Cat# 115-025-146; RRID: AB_2338488
Deposited Data		
Gene Expression Omnibus	https://www.ncbi.nlm.nih.gov/geo/	GEO: GSE107086 and GSE88954
Experimental Models: Organisms/Strains		
Mouse: PERIOD2::LUCIFERASE transgenic mice in a C57BL/6 background	[10]	N/A
Mouse: Pax2Cre mice	MMRRC	Cat# 010569-*Tg(Pax2-cre)1Akg/Mmnc*
Mouse: Bmal1flox (Bmal1$^{fx/fx}$) mice	[60]	N/A
CBA/CA/Sca mice	Scanbur—*N.B. colony has been terminated by distributor	Cat# CBSSIMA0
Software and Algorithms		
Imaris	Bitplane	http://www.bitplane.com/imaris
Lumicycle Analysis software	Actimetrics	http://www.actimetrics.com/products/lumicycle/
ClockLab	Actimetrics	http://www.actimetrics.com/products/clocklab/
Origin Software 8.1 SR1	Microcal Software	http://www.originlab.com/
BioSigRP	Tucker Davis Technologies	http://tdt.com/downloads.html
ImageJ	NIH	https://imagej.nih.gov/ij/
GraphPad Prism 6	GraphPad software	https://www.graphpad.com/
PANTHER	GeneOntology	http://www.pantherdb.org/
Other		
Millicell membrane	Millipore	PICM0RG50
Corticosterone EIA kit	Enzo Life Sciences	Cat# ADI-900-097
Square Pulse Stimulator	Grass Technologies	Cat# S44B
Stimulus RF Transformer Isolation Unit	Grass Technologies	Cat # SIU5
Stereotaxic apparatus	World Precision Instruments	Cat# 502610
CLAMS	Colombus Instruments	N/A
Running wheels	Med-Associates	Cat# ENV-044
Confocal microscope	Zeiss	Cat# 710
ABR system	Tucker Davis Technologies	Cat# Sys3
RNAlater	ThermoFisher Scientific	Cat# AM7021
Direct-zol RNA MiniPrep	Zymoresearch	Cat# R2052

(*Continued on next page*)

Continued

REAGENT or RESOURCE	SOURCE	IDENTIFIER
Bioanalyzer	Agilent	Cat# 2100
Nanostring nCounter	Nanostring technologies	N/A
Qubit fluorimeter	Life Technologies	Cat# Q33216
HiSeq 2500 sequencer	Illumina	N/A
LumiCycle Luminometer	Actimetrics	LumiCycle 32

LEAD CONTACT AND MATERIALS AVAILABILITY

Further information and requests for resources and reagents should be directed to and will be fulfilled by the Lead Contact, Christopher R. Cederroth (christopher.cederroth@ki.se).

This study did not generate new unique reagents.

EXPERIMENTAL MODEL AND SUBJECT DETAILS

All experimental procedures on animals were performed in accordance with the guidelines and regulations set forth by Karolinska Institutet and "Stockholm's Norra Djurförsöksetiska Nämnd" N370/12 and N156/14. CBA/CA/Sca mice, (from Scanbur) were used for ADX and SCN studies. PER2::LUC (*mPer2^{Luc}*) [4] and *Bmal1(fx/fx)* [61] mice were provided by Takahashi and Bradfield, respectively. *Pax-Cre* (*Pax:Cre*) mice were obtained from the MMRRC (010569-*Tg(Pax2-cre)1Akg/Mmnc*). *Bmal1(fx/fx)* mice (129SvJ × C57BL/6J N3 backcross) were crossed to *Pax2:Cre* (FVB) to produce we obtained homozygous *Bmal1(fx/fx);Pax2:Cre* as well as heterozygous *Bmal1(wt/fx);Pax2:Cre* and wild-type *Bmal1(wt/wt);Pax2:Cre* control mice (all referred as *cBmal1* mice). We further crossed *cBmal1(wt/fx);Pax2:Cre* with PER2::LUC mice (*Bmal1*;*Pax2:Cre;Per2Luc*) in order to track PER2::LUC bioluminesence from cochlear explants in presence or absence of a functional BMAL1.

All mutants were genotyped at weaning (P21) from tail biopsies by classic PCR. For *Bmal1 fx/fx* mice, we used a set of 3 primers [5436: 5-ccctgaacatgggaaagaga-3, 6013: 5-attcacctttttggggaggac-3, and 6014: 5-tcatcagaggaaccagggtaa-3] discriminating between *Bmal1 wt* (310 bp), *Bmal1 fx* (360 bp) and *Bmal1 Δ* (excised, 450 bp) alleles. For *Pax2:Cre* mice, we used a set of 2 primers [F: 5-gcctgcattaccggtcgatgcaacga-3, 16026: 5-gtggcagatggcgcggcaacaccatt-3] amplifying a Cre band at 700 bp. For PER2::LUC mice, we used a set of 3 primers [P1: 5-ctgtgtttactgcgagagt-3, P2: 5-gggtccatgtgattagaaac-3, and P3: 5-taaaaccgggaggtagatgaga-3] discriminating between WT (230 bp), LUC (680 bp) alleles.

Males aged between 2 and 4 months, were used for audiological, morphological and molecular experiments. Animals had free access water and to food (Lactamin R34, Lantmännen). Food pellets contained 43 mg/kg daidzin, 60 mg/kg genistin, 10 mg/kg glycitin, 2 mg/kg daidzein, 1.6 mg/kg genistein (Lantmännen report). Temperature was maintained between 19° and 21°C. The room lights were on at 6 a.m. and off by 6 p.m. Handling in darkness was performed in red light.

METHOD DETAILS

Adrenalectomy

After being anesthetized with an i.p. injection of ketamine (100 mg/kg) and xylazine (8 mg/kg), the adrenal glands were removed bilaterally through a dorsal midline incision and lateral retroperitoneal incisions. Following surgery, skin incisions were closed with sterile wound clips and analgesia was provided for 48h (Temgesic, 0,02 mg/ml). Starting immediately after surgery, the drinking water was replaced with 0.9% saline until the end of the experiments. Auditory threshold measures were started 2 weeks after surgery.

Corticosterone measurement

After decapitation under isoflurane anesthesia, trunk blood was collected in heparin coated tubes and placed on ice. Blood samples were centrifuged at 1400 rpm, +4°C, for 10 min and plasma was collected and placed on ice. Samples were treated with Steroid Displacement Reagent (SDR, 6 μL plasma+ 6 μL SDR) and kept at +4°C until further analysis. Feces were collected for 24 hours under LD (12 h light/12 h darkness) or 3 days in DD (24 h darkness) conditions. Metabolic cages were used to minimize handling during sample collection. Fecal collection was performed every 4th hour over 2 days. Collected samples were stored at –80°C until extracted. Blood and fecal corticosterone levels were measured with EIA kits according to the manufacturer's instructions (Corticosterone EIA kit, Enzo Life Sciences, Farmingdale, NY).

Suprachiasmatic nucleus ablations

Bilateral lesions of the SCN were performed in a stereotaxic apparatus (World Precision Instruments, Sarasota, FL) under ketamine/xylazine anesthesia (intraperitoneal injection, 80 and 14 mg/kg). A stainless steel insect pin (0.25 mm in diameter) was inserted at the following coordinates: anteroposterior, +0.5 and +0.8 mm using the bregma as the reference; lateral, ± 0.25 mm; and depth,

−5.7 mm. SCN lesions were made using a electric stimulator (S44, Grass Technologies, Warwick, RI) and stimulus isolation unit (SIU5, Grass Technologies). A 1.8 mA current was passed for 6 s. The sham lesioned mice underwent the same operation, but no electric current was passed through the electrode.

To validate the lesions, SCN lesioned (SCNx) mice and sham operated mice were individually placed in the Comprehensive Laboratory Animal Monitoring System cages (CLAMS, Columbus Instruments, Columbus, OH). After 24 h of acclimatization to the cages, animals were kept in the system for a period of at least 4 consecutive days. Respiratory metabolism was analyzed with oxygen consumption (VO_2) and respiratory exchange rate (RER). Animal movements in the horizontal or vertical directions break the infrared beams allowing for locomotor activity to be quantified [28]. The sum of any beam breakage in the horizontal direction was recorded as ambulatory movement counts (XAMB). Food intake was also assessed. Metabolic parameters and activity were analyzed separately for day (6 a.m. - 6 p.m.) and night (6 p.m. - 6 a.m.). To exclude partial lesioning of the SCN, brains of all operated mice were coronally sectioned with 14 μm thickness and stained with cresyl violet. Images were analyzed in the region between −0.22 mm and −0.82 mm, which is located caudally from the bregma along the rostro-caudal axis [62].

Actograms

To record the rhythm of locomotor activity, adult mice (at least 8-week old) were individually housed in activity wheel-equipped cages (#ENV-044, Med-Associates, St Albans City, VT) under LD 12:12 for at least 24 days. Locomotor activity was recorded using Wheel Manager sofware (#SOF-860, Med-Associates, St Albans City, VT) and analyzed using ClockLab software (Actimetrics, Wilmette, IL). Fluorescent lights (300–600 lux inside the cage) were used for behavior experiments. Mice were transferred into DD for 2 weeks. Wheel-running activity was recorded and analyzed. The free-running periods in DD and LL were calculated using $\chi 2$ periodogram analysis (Clocklab software, Actimetrics). The amplitude of circadian rhythm was analyzed using the fast Fourier transform (FFT), which estimates the relative power of approximately 24 hr period rhythm in comparison with all other periodicities in the time-series. The power spectral densities for frequencies ranging from 0 to 1 cycle/hr were determined and normalized to a total power (area under the curve) of 1.0. The peak in the circadian range (18- to 30-hr period or 0.033–0.055 cycles/hr) of the relative power was determined for each animal for comparison. If no significant periodicity in the 18–30 hr range was detected by FFT, the free-running period could not be scored. For the analysis of total daily activity, the total number of wheel revolutions per day was averaged in LD (7 first days of initial LD interval excluded) and DD.

Organotypic cultures

Adult cochleae, suprachiasmatic nucleus (SCN) and livers were dissected from PER2::LUC mice and cultured organotypically on a membrane (Millipore, PICMORG50) as described previously [23, 28]. Cochleae, dissected free of bone and stria vascularis, were kept in culture for minimum 6 days and its morphology characterized [63]. Isolated cochleae from PER2::LUC mice (6-8 weeks of age) were used. The bioluminescence emission from the cochlea was measured for a duration of 1 min every 10^{th} minute with Lumicycle, a microplate luminometer equipped with photomultiplier tubes (Actimetrics, Wilmette, IL). Parameters of PER2::LUC rhythmicity (period, amplitude and phase) were analyzed using Origin software 8.1 SR1 (Microcal Software, Northampton, MA, USA). Data from each recording trace was first normalized by subtracting the 24 h baseline drift from the raw data. The amplitude was calculated as the difference between highest (peak) and lowest (trough) photon count within one cycle. The calculation was performed from trough-to-peak and from the peak-to-trough, thus giving two values (half-cycles) within one cycle. For each amplitude data point, three half-cycles (1.5 cycle) were used for amplitude analyses. The very first peak after culture start was not used. Phase was determined as maximum (peak) luminescence between 24 and 48 hours (peak between day 1 and 2) of recording. The average peak time of each treatment group was calculated and statistically compared with the respective sham group. The period of one complete cycle was defined as the time between two consecutive peaks (i.e., the highest photon count within one cycle) and five consecutive peaks were used for averaging periods.

Drug treatment *in vivo* and *in vitro*

Ninety min prior to noise trauma, mice were given a 4 ml/kg intraperitoneal injection of 0.5 mg/kg Dexamethasone phosphate disodium salt (DEX, Sigma Aldrich, D1159) dissolved in vehicle (PBS solution). For *in vitro* treatments, we used 5 μM DEX dissolved in PBS, 50 μM Forskolin (Sigma Aldrich, F3917) dissolved in DMSO, 25μM Mifepristone (RU-486, Sigma Aldrich, M8046) dissolved in PBS or 5μM Spironolactone (Sigma Aldrich, S3378) dissolved in ethanol. PER2::LUC rhythms (amplitude and phase) were analyzed using Origin software 8.1 SR1 (Microcal Software) and period was analyzed by using the Lumicycle Analysis program from where we extracted the raw data. Data from each recording trace was first normalized by subtracting the 24h baseline drift from the raw data. The amplitude was calculated as the difference between the highest (peak) and the lowest (trough) photon count within one cycle. The calculation was performed from trough to peak and from peak to trough which gave two values (half-cycles) within a cycle. For each amplitude data point, 3 half cycles (1.5 cycles) were used for amplitude analyses. The 3 half-cycle amplitudes were then averaged in order to give the mean absolute amplitude over the selected 1.5 cycle period before and after treatment for each sample. The percentage of the amplitude change between pre-treatment and after treatment period was calculated at the end. The very first peak after culture beginning was not used. Phase was determined as the highest (peak) luminescence at around 48 hours (peak at day 2) after the start of the PER2::LUC recording of the tissue. Phase shifts were calculated in order to observe the drug effect. Phase shifts were calculated by subtracting the second peak before treatment from the first post-treatment peak, which was 12h after the trough treatment or 24h after the peak treatment. Period of one complete cycle was defined as the time between 2 consecutive peaks

(the highest photon count within one cycle). In order to define the period after treatment, more than 2 consecutive cycles were selected.

Acoustic trauma and auditory brainstem response (ABR)

To generate hearing loss, awake animals were treated with free field broadband noise at 6 - 12 kHz at intensity of 100 dB SPL for 1 h, similar to previously described noise trauma paradigm [23], at either 9 a.m. or 9 p.m. After being anesthetized with an i.p. injection of ketamine (100 mg/kg) and xylazine (10 mg/kg), auditory sensitivity was assessed with ABR thresholds for the frequency of 8, 12, 16 and 24 kHz as previously described [23]. Post-trauma measurements were performed 24h and 2 weeks after day or night exposures. Threshold shifts were determined by subtracting baseline hearing thresholds from post-exposure thresholds.

Immunocytochemistry and quantification of synaptic elements

For immunostaining, mice underwent transcardiac perfusion with 4% paraformaldehyde in phosphate-buffered saline (PBS) and cochleae were decalcified in EDTA 2% for 2-3 days. For the quantification of synaptic ribbons and synapses, surface preparations were stained for C-terminal binding protein 2 (mouse (IgG1) anti-CtBP2, 612044 from BD-Biosciences, used at 1:200), to quantify pre-synaptic ribbons and rabbit anti-Myosin VIIa, 25-6790 from Proteus Biosciences, used at 1:200 to delineate the hair cell bodies. Primary antibody incubations were performed overnight at 37oC, followed by 60-min incubations at 37oC with secondary antibodies coupled to Alexa fluor dyes (IgG1 goat anti-mouse AF568 at 1:500 and IgG donkey anti-rabbit AF647 at 1:200), correspondingly. The cochlear pieces were mounted in Vectashield, coverslipped and sealed with nail polish. Cochlear frequency mapping was then performed using a custom plug-in to ImageJ from NIH (Measure_Line.class from the Liberman laboratory at the Eaton-Peabody Laboratory). This gave the total length of the cochlea and their respective frequency points and was used as a guide obtaining confocal images for discrete frequency regions along the length of the cochlea. Confocal z stacks along discrete regions of the basilar membrane were made with a 63x oil immersion objective (N.A.1.40) on a Zeiss LSM 710 confocal microscope. A z-step-size of 642 nm was used to capture all synaptic structures of at least 10 hair cells. Image stacks were analyzed using Imaris software (x64 9.1.2, Bitplane AG, Zurich, Switzerland) for the number of ribbons as well as their volume. For assessing the total number of ribbons, surface and masking properties were identified. Then the region of interest (approximately 10 hair cells) was tagged for counting by using the ''spots'' function. After adjusting for the thresholds, puncta with pixel intensities greater than 0.7 um on an 8 bit scale (0-255) were counted. The volume of each puncta was determined by using different spot sizes function. Then the same procedure as for the number of puncta was followed in order to specify the size. The group a sample belonged to was blinded to the analyst.

mRNA extraction

To assess molecular changes in absence of entrainment, animals were placed three days in darkness (free running conditions), and decapitated under isoflurane anesthesia and organs were collected. RNA extraction was performed as previously described with slight modifications [64]. Cochleae were stored in RNAlater for 18-24 hours at 4°C prior to extraction with the Direct-zol RNA MiniPrep kit from ZymoResearch, without phase-separation (Nordic Biolabs AB, Sweden). DNase treatment was performed on-column as recommended by the manufacturer. RNA integrity was assessed using RNA 6000 nanochips with an Agilent 2100 bioanalyzer (Agilent Technologies, Palo Alto, CA) and quantity was evaluated with Nanodrop. Average 260/280 ratios were 2.05 ± SD 0.04, 260/230 ratios were 2.39 ± SD 0.39, RIN was 9.2 ± SD 0.13, and 18/28S was 2.12 ± SD 0.13.

Quantitative evaluation of mRNA transcripts

NanoString nCounter measures of mRNA transcript abundance has been validated against SybrGreen qRT-PCR assays in previous work on bacteria (R = 0.98 to 0.99) and in the cochlea (R = 0.9826 for *Per2* transcripts around the clock). NanoString nCounter assays were performed with 100 ng total RNA from 3-4 biological samples collected every 4 or 6 h around the clock as previously described [28]. Probes for the analysis were synthesized by Nanostring technologies. After probe hybridizations and Nanostring nCounter digital reading, counts for each RNA species were extracted, analyzed using a homemade Excel macro, and then expressed as counts (molecules of mRNA/sample). Barcodes were counted for – 1150 fields of view per sample. Background correction was done by subtracting the mean + 2 standard deviations of the negative controls for each sample. Values < 1 were fixed to 1. The nCounter CodeSet contained two types of built-in controls: positive controls (spiked RNA at various concentrations to assess the overall assay performance), and negative controls (alien probes for background calculation). Data handling and analysis was performed as described: background correction consisted of the subtraction of the negative control average plus two SD from the original counts.

To select adequate normalization genes from a series of candidates included in the CodeSet, their relative stability was evaluated using geNorm-method. For the final normalization of the sample values the geometric mean of the counts obtained from 6 normalization genes was calculated and used as normalization factor. Normalized quantities were averaged for three technical replicates for each data point and represented as the mean ± SD. The highest normalized relative quantity was arbitrarily designated as a value of 1.0. Fold changes were calculated from the quotient of means of these normalized quantities and reported as ± SEM.

RNA-sequencing

Total RNA was quantified with a Qubit fluorimeter (Life Technologies) and RNA integrity assessed with a Bioanalyzer (Agilent Technologies). The TruSeq mRNA stranded kit from Illumina was used for the library preparation with 300 ng of total R***N***A as input. Library molarity and quality was assessed with the Qubit and Tapestation using a DNA High sensitivity chip (Agilent Technologies). Pools of 6

libraries were loaded at 8.5 pM for clustering on a Single-read Illumina Flow cell. Reads of 50 bases for the noise experiment, or 100 bases for the around the clock experiment, were generated using the TruSeq SBS HS v3 chemistry on an Illumina HiSeq 2500 sequencer. Quality Control (QC) was done with FastQC v.0.11.5. Reads were mapped with TopHat2 v.2.0.11. Biological QC was done with PicardTools v.1.141. Reads per gene feature were counted with HTSeq v.0.6p1. Normalization was performed according to the design model with R/Bioconductor edgeR v. 3.4.2.

Noise exposure RNA-seq analysis

Three replicates for each group of animals exposed to sham noise (Sh) or noise during day (DN) or nighttime (NN), ADX or sham ADX (ShADX) [ShDNShADX, DNShADX, ShDNADX, DNADX, ShNNShADX, NNShADX, ShNNADX, NNADX], and were renamed Group 1 to 8 (Table S1) and whose cochlear tissue was collected 2h post-noise exposure were used and in total 38 samples were subjected to RNaseq. Sequencing of each replicate generated 34.7 million reads of which approximately 94% were uniquely mapped to the mouse genome and on average 27 million reads (79.82%) were uniquely mapped to known exons, allowing for gene expression level estimates.

The differential expression analysis was performed with the statistical analysis R/Bioconductor package edgeR v. 3.14.0. Briefly, the counts were normalized according to the library size and filtered. The genes having a count above 1 count per million reads (cpm) in at least 3 samples were kept for the analysis. The differentially expressed genes tests were done with a GLM (generalized linear model) with a negative binomial distribution. The raw gene number of the set is 23'420. The poorly or not expressed genes were filtered out. The genes expressed with least at 1 cpm (count per million reads) in 3 samples are kept. The differentially expressed genes p values are corrected for multiple testing error with a 5% FDR (false discovery rate). The correction used is Benjamini-Hochberg (BH). The filtered dataset consists of 15'580 genes. Of note, one of the samples of the ShDNShADX condition appeared as an outlier in a majority of genes and therefore was excluded from Figure S3 for visualization purposes, although it has been included in the statistical analysis (Data S1).

Temporal RNA-seq analysis

Three replicates for each time point (CT0, CT4, CT8, CT12, CT16 and CT20) were used and in total 36 samples were subjected to RNaseq. Sequencing of each replicate generated 33 million reads. Reads were mapped to the mouse reference genome (GRCm38/mm10) [65] using STAR 2.3.8 [66]. From all reads per sample, 86.8% to 89.2% were uniquely mapped to the genome; 9.1%–11.3% aligned to multiple loci in the genome. A custom Perl script was used to count the uniquely mapped reads for each gene (for details see [37]). The yielded count data was normalized by the size factor according to [67]. For downstream analysis such as rhythmicity assessment, visualization and clustering a variance stabilizing transformation was applied to the normalized reads.

In order to extract genes differentially expressed between ADX and sham operated mice, we used DESeq2 [67] available from the Bioconductor open development software project. For each gene, normalized counts were fit to a generalized linear model ($\sim$time + condition), where condition is the factor of interest (levels: ADX and sham operated) and time represents the different time points of the sampling (levels: CT0, CT4, CT8, CT12, CT16 and CT20). A likelihood ratio test (LRT) was subsequently applied to compare the full model with a reduced model that only includes the time factor.

In order to extract rhythmicity in gene expression of ADX or sham operated mice we applied a multiple linear regression to the data followed by a subsequent Bayesian information criterion (BIC) based model selection as described in detail elsewhere [68]. Briefly, we defined the equation $y(t) = \mu + \alpha\cos((2\pi/24\ h)t) + \beta\sin((2\pi/24\ h)t) + \text{noise}$ (where, y is the vsn stabilized expression levels for each gene, μ is the mean, t represents circadian time, α and β are the coefficients). To assess rhythmicity we defined 5 models for the two conditions (ADX and sham operated). The models differ in their value for the coefficient α and β. These coefficients determine amplitude and phase. A coefficient that is zero indicates a non-rhythmic pattern while non-zero values indicate a rhythmic pattern. Moreover, we allowed α and β to be the same for selected models for both conditions. The resulting models are defined as: Model 1 that comprises genes, which show no rhythmicity in either condition; model 2 contains genes that show rhythmicity in ADX mice only: genes that belong to model 3 show rhythmic profiles only in sham operated animals. Models 4 and 5 contain genes that are rhythmic in both conditions. While in model 5 the rhythmic parameters for amplitude and phase are different, genes categorized into model 4 share the same parameters between the two conditions. Linear regression was applied to solve all models, the model complexity was subsequently controlled by a Bayesian information criterion (BIC) based model selection (https://www.tandfonline.com/doi/abs/10.1080/01621459.1995.10476572). BIC penalizes for model complexity. We considered the resulting Schwarz weight to assess the confidence of a model and have chosen the model with the highest weight to describe the rhythmic properties. Gene expression patterns where the model selection did not reach a BIC weight (BICW) above 0.4 were categorized as ''ambiguous.'' To prove that type-I like errors (false positive) are controlled using this approach, we randomly permutated the time points within each condition of the entire RNA-Seq dataset (ADX and sham operated). The median of the ratio of type-I errors in 100 different permutations among all tested genes was 4.73% and 5.62% for ADX and sham operated, respectively. Given that rhythmic genes can vary quite strongly in gene expression between different time points, some of the permutations still might represent slightly rhythmic gene profiles for some genes and the given median is rather an overestimation. In line with this thought, at an amplitude threshold of log2fc of 0.2 the median of type-I like errors is 0.57% and 1.07% for ADX and sham operated, respectively.

Gene ontology analysis

Gene ontology analysis was performed with the ontology-based PANTHER (protein annotation through evolutionary relationship) classification system (http://www.pantherdb.org/) according to instructions [38].

QUANTIFICATION AND STATISTICAL ANALYSIS

Statistical information can be found in the figure legends of every experiment and in the respective section of the methods. If not stated otherwise statistical tests were performed in GraphPad Prism 6 (GraphPad Software, CA, USA). Where possible, all data points are shown along with mean values ± SEM unless otherwise noted. The significance level for statistical testing was set at 0.05. Reported N are the number of animals/samples analyzed.

DATA AND CODE AVAILABILITY

The RNA-Seq datasets generated during this study are available at Gene Expression Omnibus (GEO: GSE107086 and GSE88954, http://www.ncbi.nlm.nih.gov/geo/).